Skin-friction measurements in a turbulent boundary layer under the influence of free-stream turbulence

**Luis Blay Esteban · Eda Dogan · Eduardo Rodríguez-López ·
Bharathram Ganapathisubramani.**

Abstract This experimental investigation deals with the influence of free-stream turbulence (FST) produced by an active grid on the skin-friction of a zero-pressure-gradient turbulent boundary layer. Wall shear stress is obtained by oil-film interferometry (OFI). Additionally, hot-wire anemometry was performed to obtain wall-normal profiles of streamwise velocity. This enables the skin-friction to be deduced from the mean profile. Both methods show remarkable agreement for every test case. Although skin friction is shown to increase with FST; the trend with Reynolds number is found to be similar to cases without FST. Furthermore, once the change in the friction velocity is accounted for, the self-similarity of the logarithmic region and below (i.e. law of the wall) appears to hold for all FST cases investigated.

Luis Blay Esteban
Aerodynamics and Flight Mechanics Research Group, University of Southampton
E-mail: lbe1g14@soton.ac.uk

Eda Dogan
Aerodynamics and Flight Mechanics Research Group, University of Southampton
E-mail: E.Dogan@soton.ac.uk

Eduardo Rodríguez-López
Aerodynamics and Flight Mechanics Research Group, University of Southampton
E-mail: E.Rodriguez-Lopez@soton.ac.uk

Bharathram Ganapathisubramani
Aerodynamics and Flight Mechanics Research Group, University of Southampton
E-mail: G.Bharath@soton.ac.uk

1 Introduction

Free-stream turbulence (FST) exists above most of turbulent boundary layers (TBLs) encountered in natural and industrial environments, [Sharp et al., 2009]. Therefore understanding how turbulent boundary layers respond to FST is of primary importance. For a turbulent boundary layer, increasing FST is known to increase skin friction and to enhance heat transfer, [Blair, 1983, Hancock and Bradshaw, 1989]. However, a large number of previous studies focused on the correlation between the increase of skin friction and heat transfer with FST. Hancock and Bradshaw [1989] showed that the effect of FST in the turbulent boundary layer does not only depend on the turbulence intensity level but on a characteristic scale in the FST, which they defined as the dissipation length scale. However, skin-friction coefficients were deduced from logarithmic plots on the assumption that the universal logarithmic law also applies in the presence of FST. Thole and Bogard [1996] performed extensive research on FST levels up to 20% and presented boundary layer statistics that confirmed the validity of the logarithmic law in the mean profiles of the boundary layer for high turbulence levels by comparing direct measurements of total shear stress with values obtained using a Clauser fit to the log region. Similarly, Stefes and Fernholz [2004] compared skin-friction data obtained from oil film interferometry (OFI), wall hot wire and Preston tube at relatively high Reynolds numbers and FST levels up to 13%, showing that all skin-friction data points lied within an error band of approximately 6% on C_f.

Traditional indirect pressure based methods, such as the Preston tube, rely on the law of the wall and suffer from limitations arising from its intrusive nature. Velocity profile based methods such as Clauser chart are
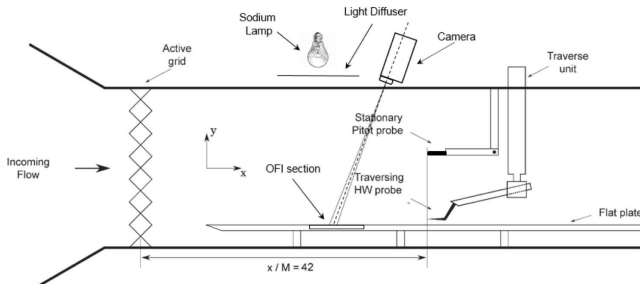
Fig. 1 Schematic of the test section illustrating hot-wire and oil-film-interferometry setup.

also of limited applicability since they also assume the existence of the law of the wall and require the knowledge of its extent and constants beforehand. Contrarily, Rodríguez-López et al. [2015] proposed to leave these constants free to adopt the value that best fits the data. In addition, this method does not require to prescribe the extent of the logarithmic layer (which can vary under FST conditions, see Dogan et al. 2016) and allows a certain uncertainty in the wall-probe initial position.

Therefore, when the validity of the universal laws are questioned, an unobtrusive, accurate and direct measurement technique to determine the wall shear stress is necessary. Several methods such as wall hot wire, OFI and floating element balance have been used during last decades for this purpose. For a comprehensive review of the available shear stress measurement techniques the reader is directed to Fernholz et al. [1996], Naughton and Sheplak [2002].

Of these available methods, OFI technique is used in this study to obtain direct measure of the wall shear stress. This technique is based exclusively on the thinning rate of a thin oil film and the forces acting on the film as flow passes over it. It only requires calibration between image-space and physical-space and can be used to obtain the wall shear stress without any knowledge or assumptions about the flow field. This technique was first introduced by Tanner and Blows [1976], who developed a simple relationship to measure shear stress by using the thin oil film equation developed by Squire [1961]. Image based technique here, is one of the several variations from the original form proposed by Tanner and Blows [1976].

2 Measurement Method and Experimental Setup

The experiments were performed at various frees-tream velocities U_∞, in an open-circuit suction type wind tunnel located at the University of Southampton. FST ranging from approximately 2% to 13% was generated by an active grid. TBL transition was promoted by the addition of a trip wire at the leading edge of the flat plate where the TBL develops. The details of the experimental setup and motor schemes of the active grid can be found in Dogan et al. [2016]. The superscript + will denote quantities normalised with the friction velocity U_τ, and the kinematic viscosity ν, as for instance in the wall-normal coordinate $y^+ = yU_\tau/\nu$, or the mean streamwise velocity $U^+ = U/U_\tau$. The details of the 28 different test cases are summarized in Table 1.

Figure 1 shows an outline of the experimental setup. OFI was used to obtain localised quantitative measurements of skin-friction velocity while a single hot-wire traversed the turbulent boundary layer up to the free stream. This study combines the merits of these two measurement techniques to compare the skin-friction coefficient ($C_f = 2U_\tau^2/U_\infty^2$) obtained from a fitting to the mean velocity profile with a direct and independent measurement technique such as OFI. Furthermore, results are compared with Preston tube measurements from Dogan et al. [2016] conducted under similar flow conditions.

The flat plate was equipped with a slot of 20×20 cm located at $x/M = 42$ downstream of the active grid (of mesh size $M = 81$ mm), where a flat glass plate was fitted. The oil (Dow Corning 200) was spread in a film with a spanwise size of 3 cm along the first quarter of the chord of the glass plate before starting the wind tunnel, so that the oil drop had sufficient space to develop into a thin film within the glass surface. The camera and the light source were mounted outside of the wind tunnel test section and the relative angle between them was recorded. The light source used was a low-pressure sodium vapour lamp with a central wavelength of approximately 590 nm. An optical diffuser was placed in front of the light source in order to provide uniform illumination for the camera field of view. The camera used was a CDD3240M monochrome camera from Thorlabs. The lens adapted to the camera was a Nikon AF Micro NIKKOR 200 mm f/4D, which gave a field of view of approximately 2.5 cm². A square grid calibration plate was used before each wind tunnel run to determine pixel-to-mm ratio. The camera was set to record images at 1 fps to obtain an accurate evolution of the thinning rate of the oil film. The oil viscosity coefficient (μ) depends on temperature and plays a relevant role in the determination of U_τ. In this study, the air temperature variation during the OFI experiments was of the order of 0.1 degrees Celsius. Therefore, the oil was assumed to be at the same temperature as the air flow inside the test section of the wind tunnel, and its viscosity was corrected accordingly.
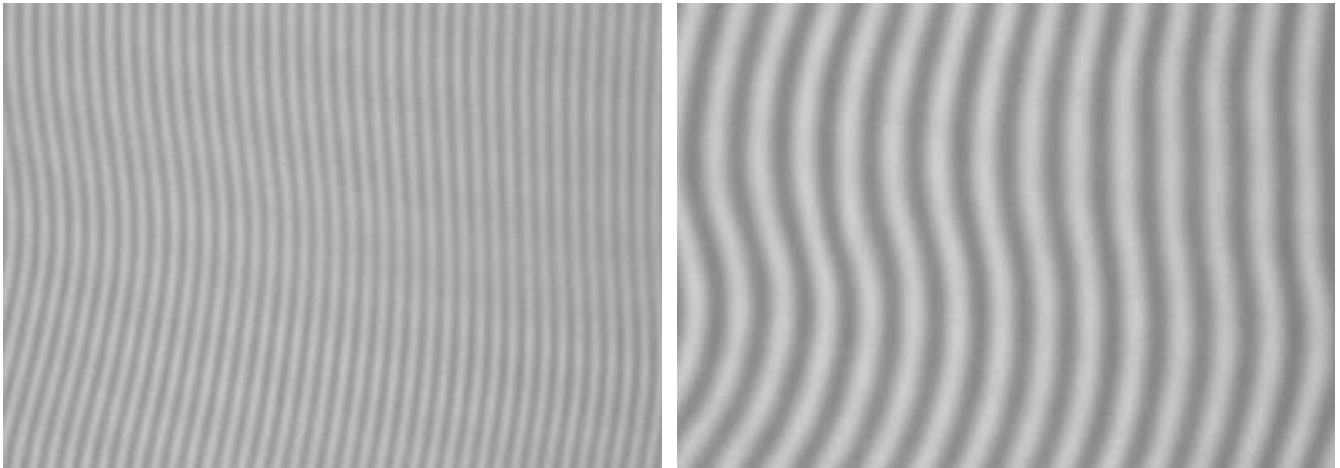
Fig. 2 Sample interferogram images, time elapsed between the two images is 300 seconds. The thin oil film is spread by the action of a turbulent boundary later under FST.

Figure 2 shows two sample interferogram images elapsed 300 s in time. An initial estimation of the distance between fringes was obtained through Fourier analysis. Then, using this result as initial guess, a sine function was fitted to the pixel intensity function so that the least-square error was minimized. Doing so, the resolution limitation inherent to the discrete Fourier transform was avoided. This is an alternative method to the use of Hilbert transform functions as proposed in Chauhan et al. [2010]. A minimum of 300 images were processed for each U_τ measurement.

The two main causes of error associated with the OFI technique are the contamination of the oil film with dust and the uncertainty in the oil properties. The presence of dust acts as noise in the periodic pattern but also changes the shape of the fringe pattern. This has the effect of changing the dominant wavelength from the analysis of the power spectrum and therefore the measured shear stress. This error was minimized by ensuring the absence of dust in the last image processed for every run. Oil properties as a function of temperature were accounted for as proposed in Zilliac [1996]. Oil viscosity was also obtained through rheometer test. The largest difference between these tests and the expression in Zilliac [1996] is found to be less than 0.9% in the kinematic viscosity of the oil.

A single 5 μm tungsten wire soldered to the copper-plated prongs of a 55P05 Dantec Dynamics anemometer was used to determine the wall-normal profiles of the streamwise velocity. The hot wire was operated using a DANTEC Streamline Pro CTA with an overheat ratio of 0.8. The motion along the wall-normal direction was carried through a traverse system. Boundary layer profile of each run involved measurements of 38 wall-normal locations, each was acquired for 3 to 5 minutes, depending on the FST and free-stream velocity, and were sampled at a rate of 20 kHz. The hot-wire was calibrated before and after each experiment.

The friction velocity U_τ, can also be determined by fitting a composite profile (U^+_{comp}) to the stream-wise mean velocity, U. This is performed following the methodology proposed by Rodríguez-López et al. [2015] in which we find the set of 5 parameters which best fit the data. These parameters are: U_τ, the uncertainty in the initial wall-probe relative position, the von Kármán constant κ, the TBL thickness δ, and the wake parameter Π. Whereas the original method considered the exponential wake [Chauhan et al., 2009] for the outer region; in the present work, we have modified the wake description following Hancock and Bradshaw [1989] to account for the effect of free-stream turbulence. The viscous, buffer and logarithmic regions are described by the Musker [1979] velocity profile such that the whole velocity description is given by

$$U^+_{comp} = U^+_{Musker}\left(y^+, \kappa\right) + \frac{1}{\kappa}\mathcal{W}\left(\frac{y}{\delta}, \Pi\right) \tag{1}$$

where

$$\mathcal{W} = (1 + 6\Pi)(y/\delta)^2 - (1 + 4\Pi)(y/\delta)^3, \tag{2}$$

implying that $\partial U^+/\partial y^+|_{y^+=\delta^+} = 0$. Note also that $U^+_{Musker}(y^+ \to 0) \to y^+$ and $U^+_{Musker}(y^+ \to \infty) \to \log(y^+)/\kappa + B$; thus recovering the viscous and logarithmic layers for small and large enough wall-normal locations respectively. The residual to be minimised is taken to be

$$E_1 = \langle\left|U^+ - U^+_{comp}\right|/U^+_{comp}\rangle, \tag{3}$$

where the $\langle\cdot\rangle$ operator represents averaging across the different wall-normal locations. This provides a larger weighting to points located close to the wall where most

of the information about the skin friction is contained. For a deeper discussion on the influence of the weighting, the reader is referred to [Rodríguez-López et al., 2015] and Kendall and Koochesfahani [2008]. Despite this method was originally validated for naturally-growing TBLs; it has been shown to perform adequately under disrupted conditions [Rodríguez-López et al., 2016, 2017]. In this case, the ability for the fit to recover the correct value of U_τ will be assessed based on $\epsilon = 100 \times (C_f^{FIT} - C_f^{OFI})/C_f^{OFI}$.

3 Results

3.1 Reynolds dependence and self-similarity

For the case of a smooth-wall zero-pressure-gradient boundary layer without FST, the skin-friction coefficient can be estimated as a function of Reynolds number based on the momentum thickness, $Re_\theta = \theta U_\infty/\nu$, through semi-empirical relations [see e.g. Nagib et al., 2007]. This relation is shown in figure 5 as a solid line. Previous studies have reported an increase in TBL skin friction under FST [Blair, 1983, Dogan et al., 2016, Hancock and Bradshaw, 1989, Stefes and Fernholz, 2004]. Figure 3 confirms this trend with increasing FST. Interestingly, we also show that the trend with Reynolds number is maintained under the influence of FST which is accounted for by a change in the offset parameter C which is a function of the FST level.
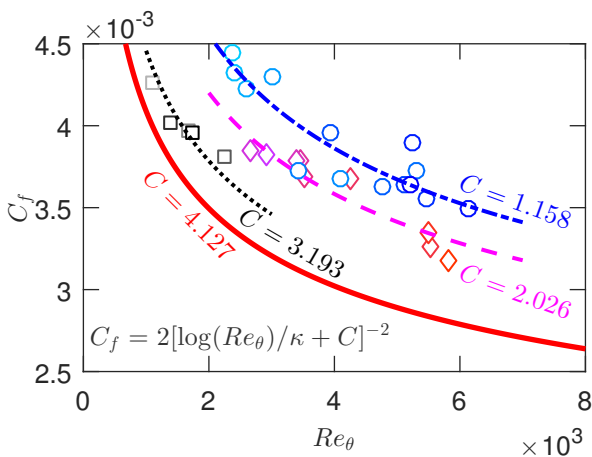

Fig. 3 Skin-friction coefficient, C_f, obtained from OFI as a function of Re_θ; squares represent low turbulence intensity cases, diamonds mid turbulence intensity cases and circles high turbulence intensity cases. Also plotted the modified Coles–Fernholz [Nagib et al., 2007] relationship for natural TBL (solid line) and fits to low (dotted line), mid (dashed line) and high (dot-dashed line) FST levels.

Similarly, figure 4 shows the same data plotted against the FST level. An increase in C_f is observed for the largest Re_θ when the FST changes from mid to high levels (i.e. from $\approx 8\%$ to $\approx 12\%$). Analogously, for cases with a similar FST level, C_f decreases as a consequence of the increase in Re_θ as shown by the arrows in figure 4. Furthermore, overall agreement is shown with the results obtained by Dogan et al. [2016] using Preston tubes for similar flow conditions.
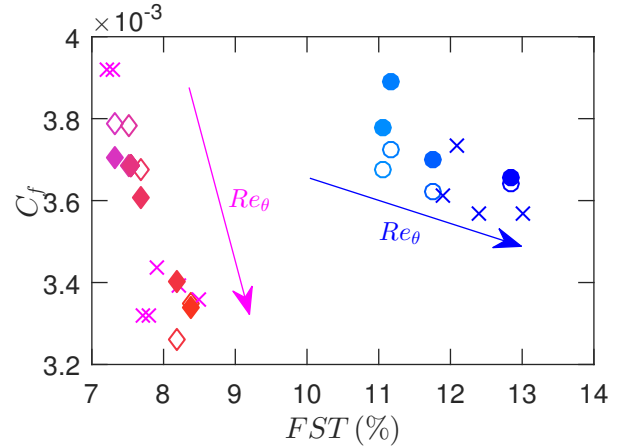

Fig. 4 Comparison between the skin-friction coefficient obtained from OFI (empty symbols), Preston tube by Dogan et al. [2016] (filled symbols) and mean-profile fitting ($\times$) techniques for similar flow conditions in the mid and high ranges of FST. The direction of the arrow represents the increase in Re_θ.

The fact that the trend followed by C_f as a function of Re_θ is similar to that of a naturally growing TBL under a laminar free stream, along with previous results [Dogan et al., 2016, Hancock and Bradshaw, 1989], suggests that the inner region of the TBL may remain self-similar under inner scaling. Moreover, it provides a further argument for the extrapolation of U_τ from the mean velocity profile (which requires the existence of a logarithmic region).

Figure 5 shows the inner-scaled mean velocity profile for all the cases summarised in Table 1. For clarity, the velocity profiles are separated in three different plots corresponding to the low, mid and high intensity FST cases. Two main conclusions can be extracted from figure 5: (i) the existence of a well-defined inner and logarithmic regions shows unequivocally that –once the change in the friction velocity is accounted for, the self-similarity of the logarithmic region and below holds for FST cases–(ii) the fitting process described above can reflect the physics of the flow both in the inner and outer layers. In fact, note that the wake region clearly differs from that expected in cases without FST where a

U_∞ (m/s)	Re_θ	δ_ν (μm)	$C_f^{OFI} \cdot 10^3$	$C_f^{FIT} \cdot 10^3$	ϵ (%)	Δ (mm)	FST (%)	$E_1 \cdot 10^3$	Symbol
4.5	1115	77.3	4.26	4.27	0.29	132.1	2.4	11.04	□
6.0	1670	59.2	3.97	4.12	3.66	138.1	2.4	9.91	□
7.6	1390	45.9	4.01	4.11	2.42	101.7	2.5	5.47	□
10.0	1751	35.4	3.96	3.85	-2.77	88.6	2.5	4.48	□
11.1	2254	32.7	3.81	3.70	-2.97	101.7	2.5	6.46	□
5.3	2674	66.7	3.85	3.91	1.61	217.8	7.2	3.44	◇
5.4	2907	65.4	3.82	3.71	-2.90	228.7	6.9	4.20	◇
6.9	3457	51.8	3.78	3.68	-2.62	200.1	7.5	3.59	◇
7.0	3393	51.3	3.79	3.70	-2.16	197.3	7.3	3.73	◇
7.0	3516	52.3	3.69	3.68	-0.10	213.8	7.5	3.40	◇
9.3	4267	39.2	3.68	3.61	-1.92	184.8	7.7	4.47	◇
12.3	5532	31.9	3.26	3.40	4.30	192.6	8.2	4.59	◇
12.4	5512	30.8	3.35	3.34	-0.38	189.5	8.4	2.66	◇
13.9	5821	28.6	3.17	3.36	5.84	184.1	8.5	3.17	◇
4.2	2380	79.1	4.44	4.31	-3.03	182.0	10.2	8.36	○
4.3	2395	78.4	4.32	4.20	-2.78	202.5	10.6	7.99	○
4.5	2593	75.1	4.23	4.08	-3.59	218.5	10.6	10.55	○
5.5	3015	61.5	4.30	4.05	-5.90	185.9	10.8	7.05	○
6.0	3414	60.8	3.72	3.89	4.46	207.5	11.2	7.59	○
6.2	4101	58.7	3.68	3.78	2.76	228.6	11.1	6.99	○
7.8	4764	47.1	3.62	3.70	2.03	225.6	11.7	5.77	○
8.0	3941	44.2	3.96	3.85	-2.64	176.9	11.8	6.14	○
8.5	5294	43.0	3.73	3.64	-2.31	227.1	11.7	7.61	○
8.7	5111	42.0	3.64	3.61	-0.81	219.1	11.9	7.99	○
9.8	5251	36.7	3.89	3.67	-5.85	182.8	12.4	5.72	○
10.5	5481	35.9	3.55	3.59	1.06	199.5	11.9	5.82	○
10.8	5220	34.2	3.64	3.66	0.39	186.3	12.8	5.09	○
11.4	6125	33.5	3.50	3.49	-0.16	200.2	12.6	7.57	○

Table 1 Experimental conditions for the 28 test cases. Note that $\delta_\nu = \nu/U_\tau^{OFI}$ and the Clauser length scale $\Delta = \delta^\star U_\tau^{OFI}/U_\infty$ where δ^* is the displacement thickness.

positive wake ($U^+ > \log(y^+)/\kappa + B$ in the wake region) is encountered; in contrast, the present cases present a negative departure. This implies that exponential wakes such as those described in Chauhan et al. [2009] cannot be used for TBLs developing under FST. Nevertheless, polynomial descriptions such as those proposed by Hancock and Bradshaw [1989] and summarised in equation 2 adequately fit the velocity profiles.

3.2 Fitting results

The self-similarity of the velocity profiles has been shown in section 3.1. Figure 5 has also shown that the method proposed by Rodríguez-López et al. [2015] can satisfactory describe the mean velocity. Despite the main aim of the fit to obtain an estimate of U_τ, it additionally provides further insight into the value of κ, δ and Π which will be discussed below.

Note that an accurate description of the wake (as shown in figure 5) presents two main advantages: it enables us to obtain δ and Π from the fitting process and it removes the need for an explicit prescription of the limits of the logarithmic layer, which could both

normally be encountered as challenges under FST conditions [Dogan et al., 2016]. Nevertheless, note that the wake's analytical description is different from that used by Dogan et al. [2016] so a straightforward comparison between their value of Π and the present ones is not possible. However, the tendency of Π to become more negative for increasingly larger FST is also captured as shown in figure 6.

Despite κ is not prescribed *a priori* in the optimisation; the values obtained from the fitting process are within reasonable limits ($0.32 \leq \kappa \leq 0.41$) of those appearing in the literature. Furthermore, larger values are consistently found for larger FST levels as shown in figure 6. In fact, for larger FST levels κ reported is closer to the recently proposed estimate of 0.39 [Marusic et al., 2013]. A possible interpretation is that the presence of FST suppresses the outer influence (or the influence of intermittency) on the logarithmic region and therefore perhaps exhibits a value that is closer to the value obtained using high Reynolds number data even at lower Reynolds numbers. In other words, the intermittency in the outer region of a natural TBL may imply a smaller value of κ for low-Reynolds flows. Should this intermittency be suppressed (by means of
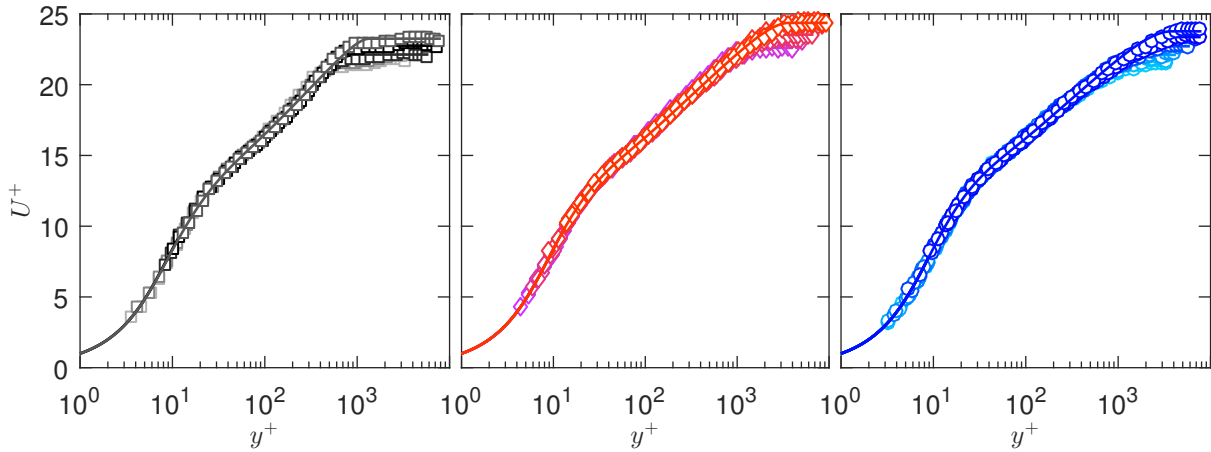
Fig. 5 Empty symbols (given in Table 1) represent the experimental inner-normalised mean velocity profile for low, mid and high intensity FST cases from left to right, respectively. The solid lines represent the fit to the mean profiles following Rodríguez-López et al. [2015].
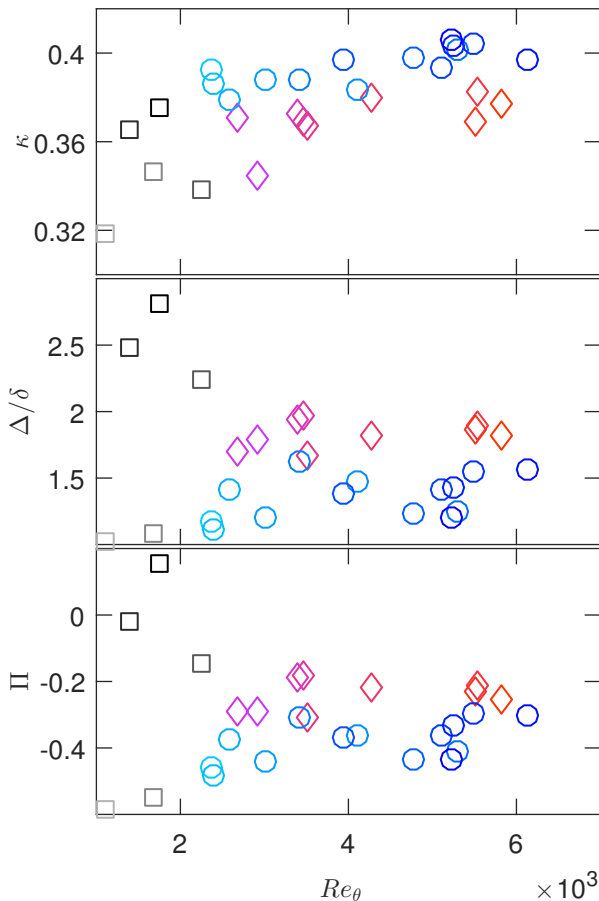

Fig. 6 Values of Π, Δ/δ and κ obtained by the fitting procedure for the 28 test cases summarised in Table 1.

increasing Re and hence scale separation or, alternatively, by the presence of FST), κ would resemble that of a high Re experiment. This would also be consistent

with the smaller value presented by the low level FST cases (black squares in figure 6).

Finally, figure 6 also shows the relationship between δ obtained from the fitting process and an integral description of the TBL thickness such as Clauser's $\Delta = \delta^{\star} U_{\tau}^{OFI}/U_{\infty}$. It is clear that for mid and high level of FST there is a clear relationship between these two definitions independent of Reynolds number. This implies that either of them can be employed for outer scaling of the velocity profiles. However, note that Δ depends on U_{τ} and U_{∞}, both of them difficult to estimate in the present experiment; whereas δ is determined independently of it.

A note of caution is required for the low level of FST cases. These are obtained by means of leaving the active grid installed but with its wings statically located parallel to the flow such that the blockage ratio is minimum. This generates very low FST levels (c.f. Table 1) but with high integral length scale. This may present important implications in the interaction with the TBL (also discussed in Dogan et al. 2016) hence the values of κ, δ and Π may be taken with caution for these cases.

3.3 C_f estimation

Apart from the descriptive values presented in section 3.2, the main advantage of the fitting proposed by Rodríguez-López et al. [2015] is the ability to extrapolate the skin friction from the velocity profile. A comparison between the values of C_f obtained by mean-profile fitting and OFI is shown in figure 7 for all the cases of the study. The two methods seem to provide consistent estimations of C_f within a 5% margin. More importantly, there seems to be no bias in any of the methods. Using
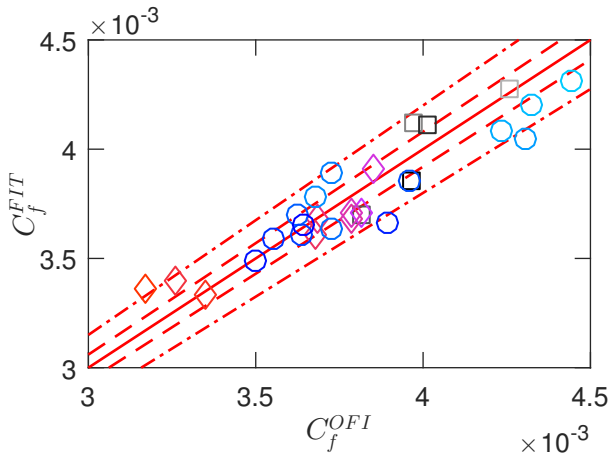
Fig. 7 Comparison between the skin-friction coefficient C_f, obtained from OFI and mean-profile fitting following Rodríguez-López et al. [2015]. (The symbols are explained in figure 3). The lines represent $C_f^{OFI} = C_f$ (solid) with 2% (dashed) and 5% (dot-dashed) margins.

$\epsilon = 100 \times (C_f - C_f^{OFI})/C_f^{OFI}$ as the relative error between the two methods. There is a negligible mean error (bias) of only 0.5% whereas the standard deviation of the 28 cases is 3.1%. Note that this dispersion accounts for possible uncertainties both in the OFI technique (camera angle, temperature, dust, etc.) and in the fitting process.

In fact, note that the dispersion of the results is uniform for the different levels of FST. More importantly, ϵ does not depend on E_1 (which measures the goodness of the fit) as can be seen by the values in Table 1. Note that both low and high FST cases present a slightly worse fit (larger E_1) which does not get reflected in a worse estimation of C_f as shown in figure 7. This robustness is significantly relevant when dealing with experimental measurements since the noise inherent to any experiment may imply a worse fit which may not necessarily result in a worse estimation of C_f.

4 Conclusions

Skin friction has been measured under FST conditions showing that the inner and logarithmic regions remain self-similar once the correct value of U_τ is obtained. C_f seems to follow a similar trend with Re_θ but increasing in a constant level with increasing FST. Analogously, κ determined by mean-profile fitting is closer to the high Reynolds number value in the presence of high FST. In addition, results from OFI and mean-profile fitting show a remarkable agreement free of any bias. Therefore, future studies should be able to use the fitting process proposed here to determine not just the skin-friction velocity but also other integral quantities such as the boundary layer thickness and the wake strength.

References

Blair MF (1983) Influence of free-stream turbulence on turbulent boundary layer heat transfer and mean profile development: part i. experimental data. Trans ASME: J Heat Transfer 105:33–40

Chauhan K, Henry CHN, Marusic I (2010) Empirical mode decomposition and hilbert transforms for analysis of oil-film interferograms. Meas Sci Technol 21:105,405

Chauhan KA, Monkewitz PA, Nagib HM (2009) Criteria for assessing experiments in zero pressure gradient boundary layers. Fluid Dynamics Research 41(2):021,404

Dogan E, Hanson RE, Ganapathisubramani B (2016) Interactions of large-scale free-stream turbulence with turbulent boundary layers. J Fluid Mech 802:79–107

Fernholz HH, Janke G, Schober M, Wagner PM, Warnack D (1996) New developments and applications of skin-friction measuring techniques. Meas Sci Technol 7:1396–1409

Hancock PE, Bradshaw P (1989) Turbulence strucure of a boundary layer beneath a turbulent free stream. J Fluid Mech 205:45–76

Kendall A, Koochesfahani M (2008) A method for estimating wall friction in turbulent wall-bounded flows. Experiments in fluids 44(5):773–780

Marusic I, Monty JP, Hultmark M, Smits AJ (2013) On the logarithmic region in wall turbulence. Journal of Fluid Mechanics 716:R3

Musker A (1979) Explicit expression for the smooth wall velocity distribution in a turbulent boundary layer. AIAA Journal 17(6):655–657

Nagib HM, Chauhan KA, Monkewitz PA (2007) Approach to an asymptotic state for zero pressure gradient turbulent boundary layers. Philosophical Transactions of the Royal Society of London A: Mathematical, Physical and Engineering Sciences 365(1852):755–770

Naughton JW, Sheplak M (2002) Modern developments in shear-stree measurement. Progress in Aerospace Sciences 38:515–570

Rodríguez-López E, Bruce PJK, Buxton ORH (2015) A robust post-processing method to determine skin friction in turbulent boundary layers from the velocity profile. Experiments in Fluids 56(4):68

Rodríguez-López E, Bruce PJ, Buxton OR (2016) On the formation mechanisms of artificially generated high reynolds number turbulent boundary layers. Boundary-Layer Meteorology 160(2):201–224

Rodríguez-López E, Bruce PJK, Buxton ORH (2017) Experimental measurement of wall shear stress in strongly disrupted flows. Journal of Turbulence 18(3):271–290

Sharp NS, Neuscamman S, Warhaft Z (2009) Effects of large-scale free stream turbulence on a turbulent boundary layer. Phys Fluids 21:095,105

Squire LC (1961) The motion of a thin oil sheet under the steady boundary layer on a body. J Fluid Mech 11:161–179

Stefes B, Fernholz HH (2004) Skin friction and turbulence measurements in a boundary layer with zero-pressure-gradient under the influence of high intensity free-stream turbulence. Eur J Mech (B/Fluids) 23:303–318

Tanner LH, Blows LG (1976) The viscosity balance method of skin friction measurement: further developments including applications to three-dimensional flow. J Phys E 9:194–202

Thole KA, Bogard DG (1996) High freestream turbulence effects on turbulent boundary layers. J Fluids Engng 118:276–284

Zilliac GG (1996) Further developments of the fringe-imagins skin friction technique. NASA Technical Memorandum pp 110425